Springer

KSME

Journal of Mechanical Science and Technology 29 (5) (2015) 2035~2045
www.springerlink.com/content/1738-494x
DOI 10.1007/s12206-015-0424-3

The reliability of finite element analysis results of the low impact test in predicting the energy absorption performance of thin-walled structures †

R. Alipour, A. Farokhi Nejad and S. Izman*

Faculty of Mechanical Engineering, Universiti Teknologi Malaysia, 81310 UTM , Johor Bahru, Johor, Malaysia

(Manuscript Received August 9, 2014; Revised February 3, 2015; Accepted February 3, 2015)

Abstract

The application of dual phase steels (DPS) such as DP600 in the form of thin-walled structure in automotive components is being continuously increased as vehicle designers utilize modern steel grades and low weight structures to improve structural performance, make automotive light and reinforce crash performance. Preventing cost enhancement of broad investigations in this area can be gained by using computers in structural analysis in order to substitute lots of experiments with finite element analysis (FEA). Nevertheless, it necessitates to be certified that selected method including element type and solution methodology is capable of predicting real condition. In this paper, numerical and experimental studies are done to specify the effect of element type selection and solution methodology on the results of finite element analysis in order to investigate the energy absorption behavior of a DP600 thin-walled structure with three different geometries under a low impact loading. The outcomes indicated the combination of implicit method and solid elements is in better agreement with the experiments. In addition, using a combination of shell element types with implicit method reduces the time of simulation remarkably, although the error of results compared to the experiments increased to some extent.

Keywords: Explicit method; Shell elements; Solid elements; Quasi-static load; Energy absorption; Thin-walled structures

1. Introduction

With increasing advances in technology, the necessity to produce designs to promote safety, particularly for transportation systems, is indispensable. In order to decrease fatalities and damage in road accidents, the need for components that can absorb collision energy and reduce damage to critical parts is necessary. Energy absorbing structures are used to reduce the undesirable effects of accidents. Energy absorbing tools fragmentize the kinetic energy of impact in the form of plastic deformation. The advantage of thin-walled structures is their low weight, low cost and simplicity of production [1].

Some important parameters for energy absorbing structures are the absorbed energy and mean crushing load which have been investigated in several previous studies. Axial loading of cylinders was first analyzed by Alexander [2] in which he introduced these structures as energy absorbers. This was followed soon afterwards with thin-walled folding tubes known as an energy absorption mechanism [1]. Based on experimental, numerical and analytical methods, various studies have investigated square and circular tubes under dynamic and quasi-static loading which can be noted in the results of Andrews et al. [3], Abramowicsz et al. [4-6].

Hanfeng et al. investigated the energy absorption characteristics of Foam-filled thin-walled structure (FTMS) by nonlinear finite element analysis through LS-DYNA [7]. The main goal of this study was to determine the most effective crashworthiness characteristics in their considered cases. Marzbanrad et al. studied a front bumper beam made of three materials: aluminum, glass mat thermoplastic (GMT) and high-strength sheet molding compound (SMC) by impact modeling to specify the deflection, impact force, stress distribution and energy-absorption behavior in order to find the best choice of material, shape and thickness [8]. Static and dynamic load tests on square-sectioned aluminum workpieces were implemented by Langseth and Hopperstad [9]. It has been shown that the mean crushing force in static mode is greater than in dynamic mode. The folds for circular and square cross-sections were similar to the load–displacement curve for folding of these tubes under axial compressive loading started with a peak and then showed oscillations. The numerical simulation and experimental investigation of behavior of circular, square, triangular and tapered sections was carried out by Alavi Nia and Hamedani [10]. Argon welding of aluminum sheets was utilized to fabricate workpieces. The effect of the weld line on the results was ignored in their simulation.

*Corresponding author. Tel.: +60 176248328
E-mail address: izman@fkm.utm.my, izman_s@yahoo.com
† Recommended by Associate Editor Jun-Sik Kim

With developments in computational methods such as finite element and widespread use of computers in engineering [11-15], experimental studies have been restricted to the essential cases and confirmation tests. In fact, FEA is used by companies throughout the world as a substitute for manually testing prototypes. With the assistance of FEA many companies and industries have decreased the time and cost of product production. FEA has also been widely implemented in the automotive industry over the past 30 years to predict the behavior of body components under condition of accidental crash events [16-19]. Although using FEA leads to reduce the cost and time of designs, the reliability of results especially in the area of automotive which involve human life is essential. One of the most important parameters contributing to the mentioned reliability is to select the finite element method (FEM) including the element types and solution methodology.

There are three general viewpoints correlated to the selection of element type particularly for simulating behavior of thin-walled structures forced to crash. The first is to utilize beam elements [20-22]. However, beam elements have a simple structure such that modeling of some effective parameters such as welding zones is practically impossible. In addition, as mentioned earlier, folding mechanism is a method to study the energy absorption phenomenon which cannot be observed using beam elements in the simulation. Therefore, beam elements are not used in this study. The second option is to employ shell elements [23-25] and the third consists of applying solid elements [26-28].

Considering energy absorption via impact loading has a dynamic nature [29], dynamic solution methodology is always employed in simulation. Briefly, in the case of the dynamic approach, implicit and explicit solution methods [1, 10, 30, 31] are the general categories of dynamic methodology in FEA considering the conventional uniform time-stepping schemes. However, in some cases [32, 33] a combination of mentioned methods has been used. The implicit methods mainly consist of the midpoint algorithm and the backward Euler scheme [34]. The explicit methods generally address the forward Euler scheme [35] and Runge–Kutta scheme [36]. They are normally facilitated by the sub-incrimination technique [37] or algorithms helping to return the stress state to the yield surface [38].

In the present paper, the effect of element formulation and solution methodology on simulation of low impact test in predicting the energy absorption in the form of thin-walled tubes with simple sections are investigated. The category of elements selected are consist of shell and solid. The solution methodology is implemented based on implicit and explicit. To validate the numerical results three kinds of samples with different thicknesses and sections are experimented. The peak load and energy absorption of samples resulted from load-displacement curves are evaluated as the parameters of validation. In the final step of study, run time of all numerical simulations is considered.

2. Experimental study

2.1 Material and geometry of specimens

The samples were a type of square cross-section made from

Table 1. Mechanical properties of samples.

Property	Value		
	DP600	Welded zone	HAZ
Young module (GPa)	207	210	210
Yield strength (MPa)	417	642	801
Ultimate strength (MPa)	818	1637	1309

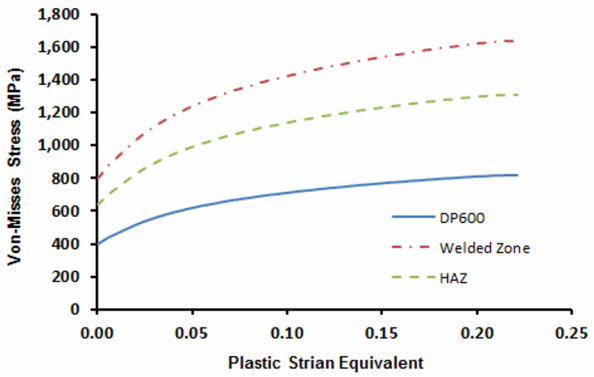

Fig. 1. Stress–strain curve for DP600, welding zone and HAZ.

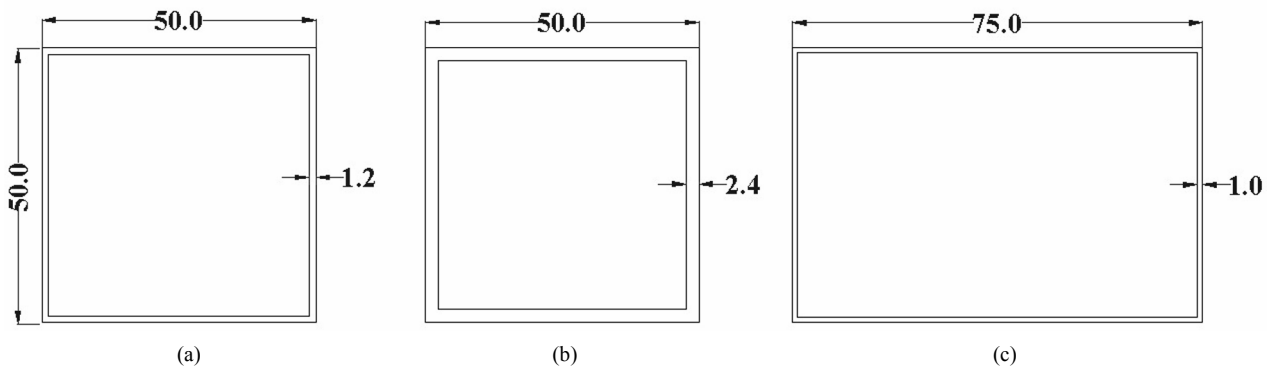

Fig. 2. Section geometry and dimensions of specimens.

Table 2. Code of samples.

Geometry of specimens		Codes	
Cross section size	Thickness	Specimen 1	Specimen 2
50 x 75 mm	1 mm	LT-1	LT-2
50 x 50 mm	1.2 mm	MT-1	MT-2
50 x 50 mm	2.4 mm	HT-1	HT-2

Fig. 3. Instron 600KN machine.

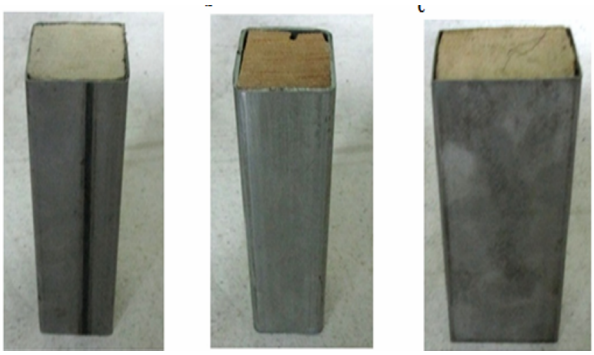

(a) (b) (c)

Fig. 4. Cross section of samples before experiments: (a) 1.2 mm; (b) 2.4 mm; (c) 1 mm thickness.

1, 1.2 and 2.4 mm thick DP600 sheets. The DP600 sheet was cut using wire-cut machine to the desired dimensions and friction welding method was used to connect the edges. The mechanical properties of the welded zone and heat affected zone were determined in order to use in simulations. The mechanical properties of the specimens were specified based on ASTM E8M standards [39]. The stress–strain curve of the base metal (DP600), welded zone and HAZ are shown in Fig. 1 and the mechanical properties are presented in Table 1. The height of samples were 150 mm. The dimension of cross-sections were 50 mm x 50 mm and 50 mm x 75 mm. Section geometry of specimens are shown in Fig. 2.

2.2 Experiments

Quasi-static loading of samples was implemented utilizing an Instron 600KN machine as shown in Fig. 3. This device has two jaws; top is movable and the lower is fixed.

The compressive axial loading velocity was set to 10 mm/min. Small force was required to compress the workpiece because of being thin-walled. In order to avoid slippage of the specimens, wood was located in the inputs of cross-sections. A simple code was assigned to each specimen. Table 2 displays the mentioned codes. Fig. 4 shows the cross-section of specimens before experiments. The deformed samples after experiments are shown in Fig. 5. In order to ensure correct responses, the tests were replicated twice.

3. Finite element analysis

Finite element simulations to axial compressive test of the thin-walled structures were carried out employing ABAQUS software. A discrete rigid part was used for the jaws. Shell and solid elements for the samples were applied. Johnson-cook material model was used for specimens which is purely empirical and gives the Eq. (1) for the flow stress [40-42].

$$\sigma(\varepsilon,\dot{\varepsilon},T)=\left[A+B(\varepsilon)^{n}\right]\left[1+C\ln(\dot{\varepsilon}^{*})\right]\left[1-(T^{*})^{m}\right] \quad (1)$$

where ε is the equivalent plastic strain, $\dot{\varepsilon}$ is the plastic strain-rate, T is temperature, and A, B, C, n, m are material constants. The normalized strain-rate and temperature in Eq. (1) are expressed as

$$\dot{\varepsilon}^{*}=\frac{\dot{\varepsilon}}{\dot{\varepsilon}_{0}} \quad (2)$$

$$T^{*}=\left(\frac{T-T_{0}}{T_{m}-T_{0}}\right). \quad (3)$$

In Eq. (2), $\dot{\varepsilon}_{0}$ is the effective plastic strain-rate of the quasi-static test used to determine the yield and hardening parameters A, B and n. In Eq. (3), T_{0} is a reference temperature, and T_{m} is a reference melt temperature. The parameters of Johnson-cook equation for DP600, welded zone and HAZ have been identified [43] and displayed in Table 3.

The lower jaw was stationary and the upper one moved downward with a speed equal to 10 mm/min, as same as experiments. Similar boundary conditions and loading method were applied to all samples. A couple of reference points were defined for rigid jaws to allocate the boundary conditions. As well, a couple of surfaces were defined at the top and down of specimens for applying boundary conditions. Upper jaw and specimens were fixed in all degree of freedoms except for along loading direction in order to avoid slippage as same as using wood in experiments. The lower jaw was fixed in all degrees of freedom.

It is worth remarking that the accuracy of a material nonlinear analysis, such as energy absorbing too much depends on

the integration strategy employed to integrate the rate equations, and previous researchers have suggested various types of algorithms for this determination. These algorithms can be categorized into explicit and implicit categories [30]. Both of implicit and explicit solution were done for simulation. The mesh convergence test was implemented for all models to find optimum size of mesh. Several types of shell and solid elements provided by ABAQUS were employed in the simulations. Fig. 6 shows a sample of Abaqus assembled and meshed models. More details about simulation are given in the following sections.

Table 3. The parameters of Johnson-cook equation for specimens.

Parameters	Material		
	DP600	Welded zone	HAZ
A (MPa)	350	642	801
B (MPa)	902	1812	2187
C	0.0144	0.049	0.047
m	1.23	1.34	1.47
n	0.189	0.187	0.19

3.1 Implicit method

In this paper, the term called implicit is diverted to the method in which the state of a FEM is updated from time t to $t + \Delta t$. It means in a fully implicit procedure the state at $t + \Delta t$ is determined based on data at time $t + \Delta t$. Despite the explicit strategy uses data at time t to solve for $t + \Delta t$. ABAQUS/standard utilizes a form of the Newton–Raphson iterative solution method [44] to solve for the incremental set of equations which is presented as underlined. In the case of the quasi-static boundary value problem approach, a set of

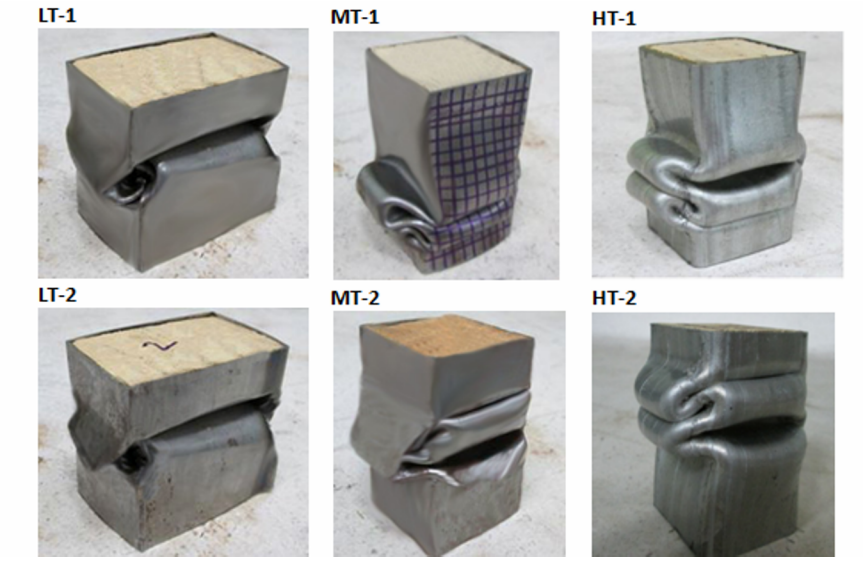

Fig. 5. Deformed samples after experiments.

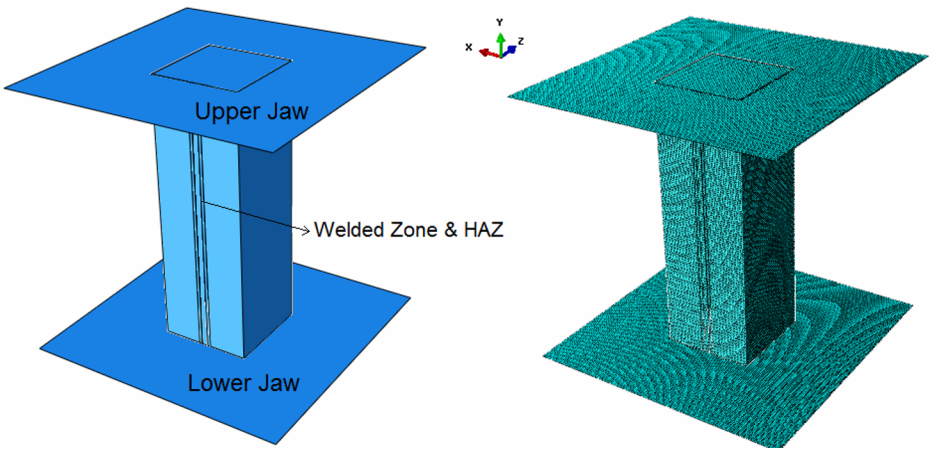

(a) (b)

Fig. 6. A Sample of FEM tubes and jaws; assembled (a); and meshed (b).

non-linear equations is assembled [45]:

$$G(u) = \int_V B^T \sigma(u) dV - \int_S N^T t dS \tag{4}$$

where u is the vector of nodal displacements and G is a set of non-linear equations with u. B is the matrix relating the strain vector to displacement. σ is the stress vector. The product of B^T and σ is integrated over a volume, V. N is the matrix of element shape functions which is integrated over a surface, S. The surface traction vector is denoted by t. Incremental methods are generally used to solve Eq. (4), where loads/displacements are applied in time steps, Δt, up to an ultimate time, t.

During updating the state of the analysis incrementally from time t to time $t + \Delta t$, an estimation of the roots of Eq. (4) is determined. For the iteration number i:

$$\delta u_{i+1} = u_{i+1}^{t+\Delta t} - u_i^{t+\Delta t} = -\left[\frac{\partial G(u_i^{t+\Delta t})}{\partial u}\right]^{-1} G(u_i^{t+\Delta t}) . \tag{5}$$

In Eq. (5), $u_i^{t+\Delta t}$ refers the vector of nodal displacements at time $t + \Delta t$ for the iteration number i. The term in the bracket is the Jacobian matrix of the governing equations and can be addressed to as K or the global stiffness matrix. Eq. (5) is manipulated and turn to establish a system of linear equations:

$$K(u_i^{t+\Delta t}) = -G(u_i^{t+\Delta t}) . \tag{6}$$

If δu_{i+1} is considered as the incremental displacements, Eq. (6) need to be solved for whole iterations, for the change in δu_{i+1}. Obviously, to solve for δu_{i+1}, K need to be inverted.

3.2 Explicit method

The early philosophy of developing explicit method is to solve dynamic problems associated with deformable bodies. No need for solving a system of equations or involving any iterative procedure in each time step is the most significant specification of explicit methods [46], whereupon far less computation is required per time step. Subsequently, implementation of explicit methods will be more comfortable. In fact, during a time increment, velocities and accelerations at a particular point in time are assumed to be constant and are utilized to solve for the next point in time [45]. ABAQUS/explicit employs a forward Euler integration scheme as follows [44]:

$$u^{(i+1)} = u^{(i)} + \Delta t^{(i+1)} \dot{u}^{(i+\frac{1}{2})} \tag{7}$$

$$\dot{u}^{(i+\frac{1}{2})} = \dot{u}^{(i-\frac{1}{2})} + \frac{\Delta t^{(i+1)} + \Delta t^{(i)}}{2} \ddot{u}^{(i)} \tag{8}$$

where u and superscripts refer to the displacement and the time increment respectively. In fact, the state of the analysis is advanced by assuming constant values for the velocities, $\dot{u}$, and the accelerations, $\ddot{u}$, across half time intervals. The accelerations are calculated at the start of the increment by [45]:

$$\ddot{u}^{(i)} = M^{-1} \cdot (F^{(i)} - I^{(i)}) \tag{9}$$

where F is the vector of externally applied forces, I is the vector of internal element forces and M is the lumped mass matrix. As the lumped mass matrix is diagonalised it is a trivial process to invert it, unlike the global stiffness matrix in the implicit solution method.

3.3 Shell elements

Shell elements in ABAQUS are generally divided into three categories consisting of general-purpose (SH-GP), thin (SH-T), and thick shell elements [47]. Results offered by thin shell elements are defined by classical Kirchhoff shell theory [48], while thick shell elements are modeled by shear flexible Mindlin shell theory [49]. The third group is general-purpose shell elements which can provide solutions to both thin and thick shell problems. All shell elements use bending strain measures that are approximations to those of Koiter-Sanders shell theory [50]. Although ABAQUS/Standard is capable to use shell elements in all mentioned categories, nevertheless, ABAQUS/Explicit provides only for a part of general-purpose shell elements [47].

Whereas the nature of the problem which is presented in this paper is related to the thin-walled structures, The thin and general-purpose shell elements are used for simulations.

3.4 Solid (Continuum) elements

The solid elements which are in ABAQUS all are able to be applied for finite strain and rotation in large-displacement analysis. They are the standard volume elements of Abaqus and do not include structural elements such as beams and shells. The solid elements can be composed of a single homogeneous material or, in ABAQUS/Standard, can include several layers of different materials for the analysis of laminated composite solids. Entitlement more accuracy if not distorted, particularly for quadrilaterals and hexahedra elements has been made them as a common type of elements for FE users [47]. Regarding the case of problem hexahedra solid elements were selected for simulations.

3.5 Simulations

Based on Secs. 3.1 to 3.4 several simulations were carried out. A simple code was assigned to each simulation. Table 4 displays the mentioned codes. Codes for the simulations are as follows: 1.2 mm thickness (MT), 2.4 mm thickness (HT) and 1 mm (LT). For Element types thin shell, general purpose

Table 4. Code of simulations based on element types and solution methods.

Geometry of specimens		Codes					
		Thin shell elements		General purpose shell elements		Solid elements	
Cross section	Thickness	Implicit	Explicit	Implicit	Explicit	Implicit	Explicit
50 x 50 mm	1.2 mm	MT-SH-T-I	-	MT-SH-GP-I	MT- SH-GP-E	MT-S-I	MT-S-E
50 x 50 mm	2.4 mm	HT-SH-T-I	-	HT-SH-GP-I	HT- SH-GP-E	HT-S-I	HT-S-E
50 x 75 mm	1 mm	LT-SH-T-I	-	LT-SH-GP-I	LT- SH-GP-E	LT-S-I	LT-S-E

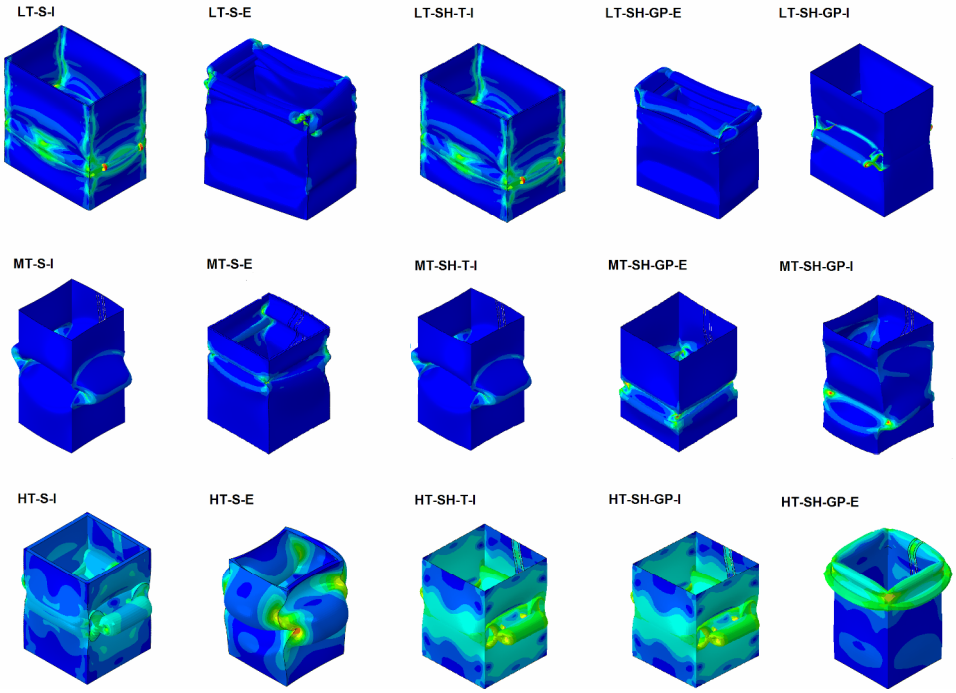

Fig. 7. Deformation modes of various samples after loading obtained from simulations.

shell and solid codes are denoted by (SH-T), (SH-GP) and (S) respectively. For implicit and explicit methods (I) and (E) are assigned in the end of codes respectively. The simulated specimens after deformation are shown in Fig. 7. The deformed simulated samples are shown in Fig. 7.

4. Results and discussion

The goal of design of axial crushing is to provide a controllable crushing pattern for maximizing energy absorption and allowable peak forces during the collapse. There are several indicators to evaluate the crashworthiness of axial crushing of a structure. Energy absorption (*EA*), specific energy absorption (*SEA*), average crush force (F_{avg}), peak force (F_{max}), and crush force efficiency (*CFE*) are broadly used in measuring crashworthiness [51]. The load - displacement curve is an useful device to extract the above-mentioned indicators. Fig. 7 is a schematic of the load - displacement curve in which the mentioned crashworthiness parameters have showed.

In this study, F_{max} and *EA* have been selected to evaluate the reliability of FEA results. Considering the recent parameters the value of *SEA*, F_{avg} and *CFE* are computable [51]. The F_{max} is addressed to the load required to initiate collapse whereupon the energy absorption process is started [52] as in Fig. 8. The *EA* specifies the stable limit of a structure and assists to compare the various designs [51]. The absorbed energy, during the axial compression is determined by integration of the load versus displacement curve shown in Fig. 8. Thus, *EA* of a sample is formulated as Eq. (10).

$$EA = \int_0^{\delta} F(\delta) d\delta \tag{10}$$

where $F(\delta)$ is the instantaneous crushing force corresponding the displacement of δ. The instantaneous crushing load can be obtained from experiments or simulation. Load–displacement diagrams of samples obtained from experiments and simulations are shown and compared in Figs. 9-11.

The overview of load-displacement diagrams implies that all the simulation methods are able to predict the samples behavior during the experiments to some extent. Aside from P_{max} which is the greatest value, there are some smaller peaks on the some diagrams. These peaks display the secondary folds

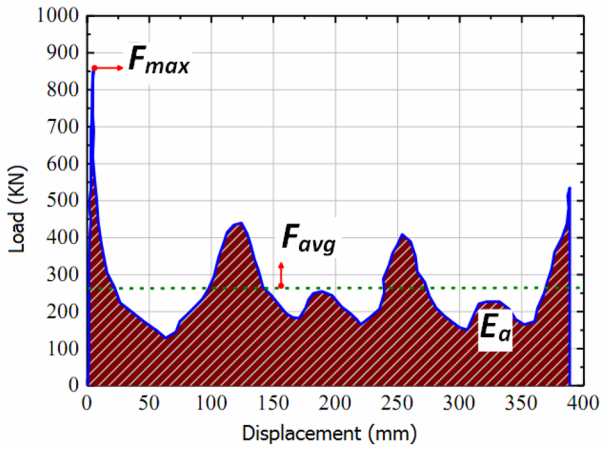

Fig. 8. Schematic of load-displacement curve to show the relationship of force versus displacement of axial crushing behavior with progressive folding.

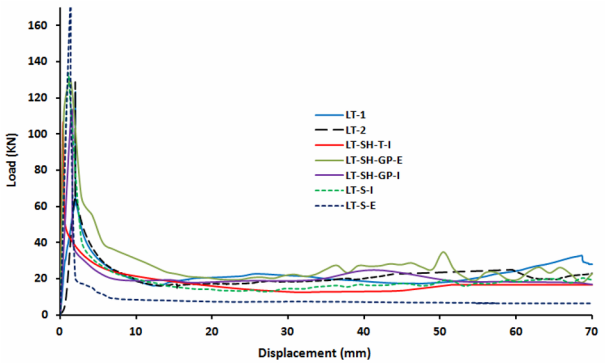

Fig. 9. Load displacement curve for the sample 50 x 75 mm cross section and 1 mm thickness.

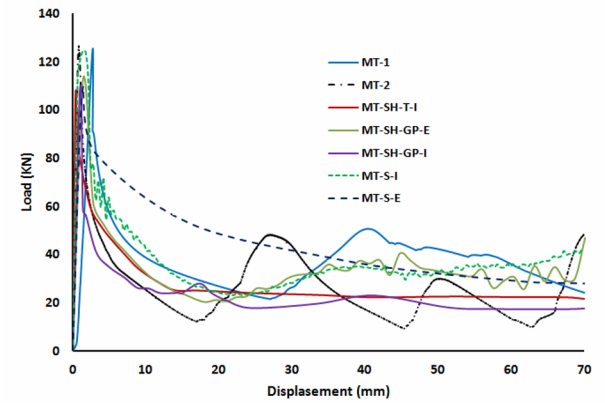

Fig. 10. Load displacement curve for the sample 50 x 50 mm cross section and 1.2 mm thickness.

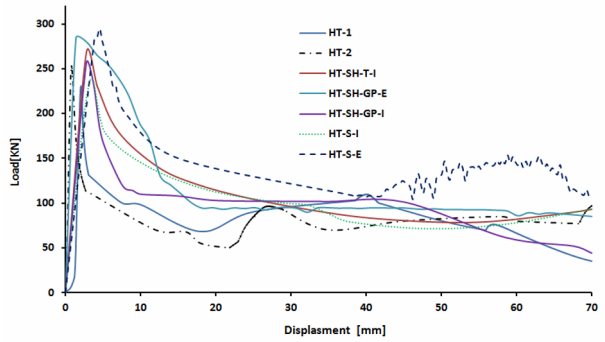

Fig. 11. Load displacement curve for the sample 50 x 50 mm cross section and 2.4 mm thickness.

on the samples. Previous researches indicate that neglecting the effect of fabrication method in simulation approaches, leads to remarkably higher peak loads compared to experiments [1]. Therefore, in present study the effect of welded zoon and head affected zoon are considered in the simulations. Brief surveys of load-displacement diagrams show that generally the implicit method can be in better agreement with experiments in comparison to explicit method. While in some cases such as Refs. [1, 7, 10] explicit method has been employed to investigate these type of problems. It seems the main reason of using the explicit approach as opposed to the implicit is to avoid convergence problems [31]. Also, it is worth mentioning that some commercial software such as LS-DYNA only employs the explicit solvers. However, ABAQUS has been equipped with quasi-static module on its implicit solver.

Figs. 12-17 show and compare the value of P_{max} and AE respectively for experiments and simulations.

These figures show that the P_{max} and AE estimated by the combination of solid elements and implicit method are more precise in comparison to the experiments. Nevertheless, the results of P_{max} and AE obtained by the implicit method and SH-GP elements are closer to the combination of solid elements and implicit methods in comparing to other combinations which have been employed in this field. Moreover, outcomes show with increase in thickness of experimental samples, better accuracy is reached from the simulations in which the solid elements are applied, provided that employing implicit method. Although the results obtained from the combination of solid elements and implicit method in all simulations has a minimal error in comparison with experiments, however decreasing the samples thickness lead to increase in result precision obtained from combination of SH-GP elements and implicit method. Thinning out the thickness of samples, their behavior become more conformed to the shell structures. That might be a reason why SH-GP elements present more accurate solution to predict the behavior of samples in this condition. Also, Figs. 12-17 show that the combination of solid elements and explicit methods does not follow a specific trend to predict the behavior of samples nor in P_{max} and neither in EA criteria.

The results obtained from combination of SH-T elements is with implicit method is close to combination of SH-GP with implicit method to some extent. Nonetheless, as Figs. 12-17 show SH-GP elements provide the more accurate solutions in

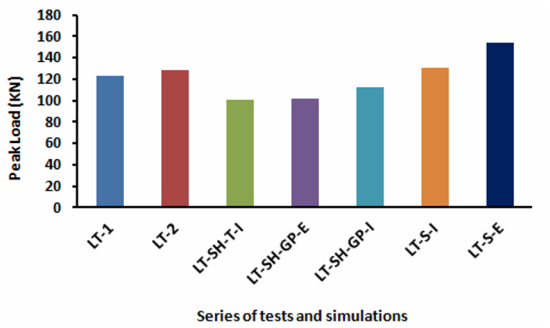

Fig. 12. Comparison between experimental and numerical peak loads for the sample 50 x 75 mm cross section and 1 mm thickness.

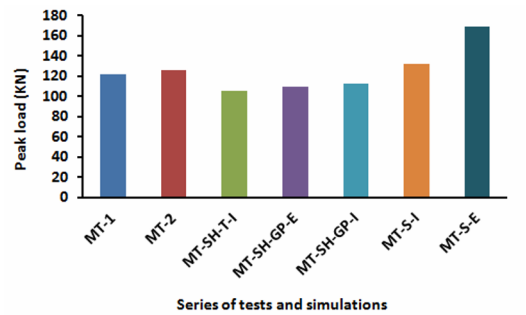

Fig. 13. Comparison between experimental and numerical peak loads for the sample 50 x 50 mm cross section and 1.2 mm thickness.

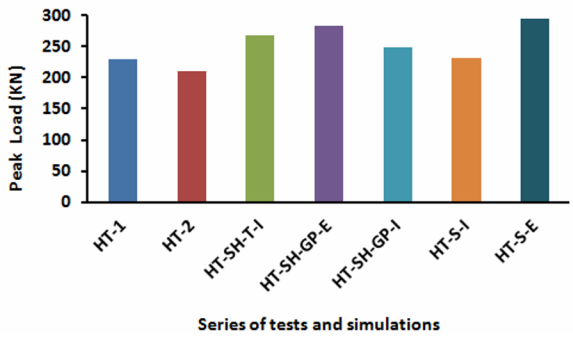

Fig. 14. Comparison between experimental and numerical peak loads for the sample 50 x 50 mm cross section and 2.4 mm thickness.

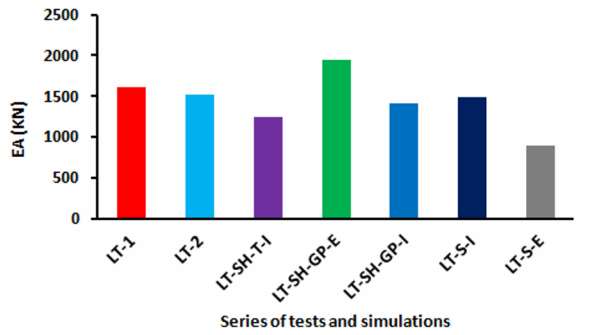

Fig. 15. Comparison between experimental and numerical *EA* for the sample 50 x 75 mm cross section and 1 mm thickness.

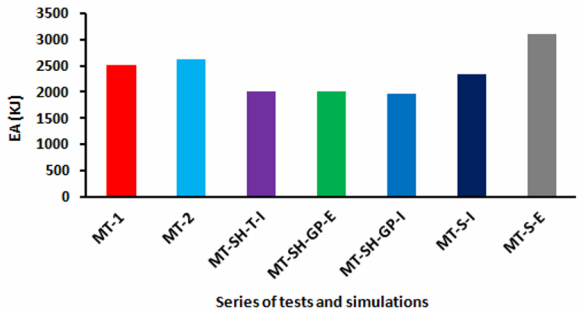

Fig. 16. Comparison between experimental and numerical *EA* for the sample 50 x 50 mm cross section and 1.2 mm thickness.

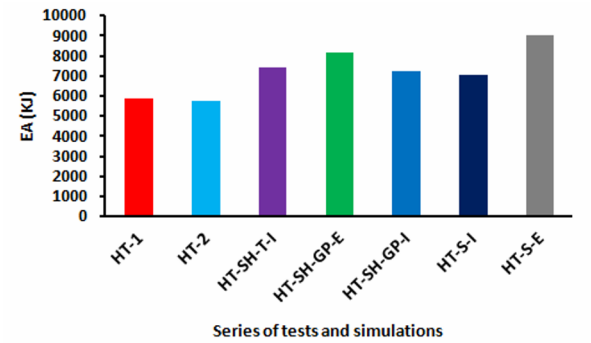

Fig. 17. Comparison between experimental and numerical *EA* for the sample 50 x 50 mm cross section and 2.4 mm thickness.

comparison to the general purpose shell elements. The recent result seems reasonable considering the overview of SH-T and SH-GP elements. Because the SH-GP elements are well-suited for many impact dynamics problems, including structures undergoing large-scale buckling behavior. Whereas, the SH-T elements is designed for modeling of thin structures that exhibit at most weak nonlinearities in problems where rotation degree of freedom output is not required and for situations where the shell surface and the displacement field are smooth [47].

One of the most important issues in FEA is to reduce the cost of analysis, including time of solution so that in some cases the users need to switch on multi time-stepping schemes [53]. However, using the mentioned schemes is required for high-experienced and advanced users of FE software. So, despite existing the multi time-stepping schemes employing the conventional uniform time-stepping schemes are still customary. When a structure is simple, the time of solution is short and its importance does not seem substantial. But, it is worth mentioning that complicated structures such as lightweight automotive platforms come from the accumulation of the mentioned simple structures and thus the time and cost of simulations increase in parallel of complexity.

There are several possible indicators can be considered to study time of simulations. Run time [53], wall-clock time [54], run-time per iteration [55] and CPU time [56] are the examples of these indicators. Run time indicator is an appropriate

Table 5. Computer specifications and conditions.

CPU	Intel Core i5, 3.1 GHz
RAM	12 GB
Graphic card	Geforce GT 630, 2 GB
Operation system	Windows 7, professional edition

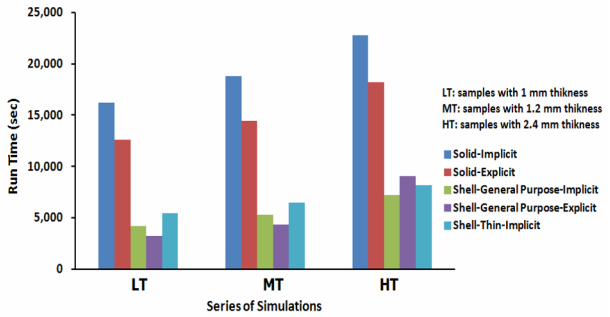

Fig. 18. Computational runtimes for different simulation methods.

parameter to study provided that the simulations are run by a same computer. Computer specifications used in the present study are listed in Table 5. Details of actual runtimes for the different solution methods are depicted in Fig. 18.

Fig. 18 shows while the use of combination of solid elements with the implicit method in conjunction with the present type of problem allows the user to obtain a simulation with minimal error, however it increases the time of simulation. In better word, the cost of simulation increases dramatically. Whereas using the combination of SH-GP elements with implicit method reduces the time of simulations up to 75%, depending on geometry, although the error percentage increases to some extent. The main reason of time reduction by employing SH-GP elements is to use simplified methods for strain calculation and hourglass control so that they offer significant advantages in computational speed [44].

5. Conclusions

In this paper, the effect of element type and solution methodology were studied on the FEA results of thin-walled structures subjected to quasi-static loading. Simulations were done using ABAQUS code and samples were loaded using an Instron apparatus. For simulations, five combinations including element types and solution methodology were implemented. Results showed partly good consistency between all the simulation methods and experiments. In the meantime, the combination of implicit method and solid elements for all simulations was in better agreement with the experiments for both of peak load and energy absorption criteria. On the other hand, combination of SH-GP elements with implicit method for all simulations was in the second rank of agreement with experimental results and decrease the time of simulations up to 75% dependent on geometry.

References

[1] A. A. Nia and M. Parsapour, Comparative analysis of energy absorption capacity of simple and multi-cell thin-walled tubes with triangular, square, hexagonal and octagonal sections, *Thin-Walled Structures*, 74 (2014) 155-165.

[2] J. M. Alexander, An approximate analysis of the collapse of thin cylindrical shells under axial loading, *Mech. Appl. Math*., 13 (1960) 5-10.

[3] K. R. F. Andrews, G. L. England and E. Ghani, Classification of the axial collapse of cylindrical tubes under quasi-static loading, *International Journal of Mechanical Sciences*, 25 (1983) 687-696.

[4] W. Abramowicz and N. Jones, Dynamic axial crushing of square tubes, *International Journal of Impact Engineering*, 2 (1984) 179-208.

[5] W. Abramowicz and N. Jones, Dynamic progressive buckling of circular and square tubes, *International Journal of Impact Engineering*, 4 (1986) 243-270.

[6] W. Abramowicz and T. Wierzbicki, Axial Crushing of Multicorner Sheet Metal Columns, *Appl. Mech. – Trans. ASME*, 56 (1989) 113-120.

[7] H. Yin, G. Wen, Z. Liu and Q. Qing, Crashworthiness optimization design for foam-filled multi-cell thin-walled structures, *Thin-Walled Structures*, 75 (2014) 8-17.

[8] J. Marzbanrad, M. Alijanpour and M. S. Kiasat, Design and analysis of an automotive bumper beam in low-speed frontal crashes, *Thin-Walled Structures*, 47 (2009) 902-911.

[9] M. Langseth and O. S. Hopperstad, Static and dynamic axial crushing of square thin-walled aluminium extrusions, *International Journal of Impact Engineering*, 18 (1996) 949-968.

[10] A. A. Nia and J. H. Hamedani, Comparative analysis of energy absorption and deformations of thin walled tubes with various section geometries, *Thin-Walled Structures*, 48 (2010) 946-954.

[11] H. Shyh-Chour, Biomechanical modeling and simulations of automobile crash victims, *Computers & Structures*, 57 (1995) 541-549.

[12] S. W. Gong, H. P. Lee and C. Lu, Computational simulation of the human head response to non-contact impact, *Computers & Structures*, 86 (2008) 758-770.

[13] C. Dørum, O.-G. Lademo, O. R. Myhr, T. Berstad and O. S. Hopperstad, Finite element analysis of plastic failure in heat-affected zone of welded aluminium connections, *Computers & Structures*, 88 (2010) 519-528.

[14] F. Szmytka, M. H. Maitournam and L. Rémy, An implicit integration procedure for an elasto-viscoplastic model and its application to thermomechanical fatigue design of automotive parts, *Computers & Structures*, 119 (2013) 155-165.

[15] M. Palmonella, M. I. Friswell, J. E. Mottershead and A. W. Lees, Finite element models of spot welds in structural dynamics: review and updating, *Computers & Structures*, 83

(2005) 648-661.
[16] I. T. Pearson and J. T. Mottram, A finite element modelling methodology for the non-linear stiffness evaluation of adhesively bonded single lap-joints: Part 1, Evaluation of key parameters, *Computers & Structures*, 90-91 (2012) 76-88.
[17] A. B. Pifko and R. Winter, Theory and application of finite element analysis to structural crash simulation, *Computers & Structures*, 13 (1981) 277-285.
[18] T. Belytschko, On computational methods for crashworthiness, *Computers & Structures*, 42 (1992) 271-279.
[19] H. Garnet and A. B. Pifko, An efficient triangular plate bending finite element for crash simulation, *Computers & Structures*, 16 (1983) 371-379.
[20] E. Carrera and A. Pagani, Analysis of reinforced and thin-walled structures by multi-line refined 1D/beam models, *International Journal of Mechanical Sciences*, 75 (2013) 278-287.
[21] A. Y. T. Leung, Non-conservative dynamic stiffness analysis of thin-walled structures, *Computers & Structures*, 48 (1993) 703-709.
[22] E. Carrera and A. Varello, Dynamic response of thin-walled structures by variable kinematic one-dimensional models, *Journal of Sound and Vibration*, 331 (2012) 5268-5282.
[23] E. Wyart, D. Coulon, T. Pardoen, J. F. Remacle and F. Lani, Application of the substructured finite element/extended finite element method (S-FE/XFE) to the analysis of cracks in aircraft thin walled structures, *Engineering Fracture Mechanics*, 76 (2009) 44-58.
[24] J. Z. Li, K. C. Hung and Z. Z. Cen, Shell element of relative degree of freedom and its application on buckling analysis of thin-walled structures, *Thin-Walled Structures*, 40 (2002) 865-876.
[25] W. Abramowicz, Thin-walled structures as impact energy absorbers, *Thin-Walled Structures*, 41 (2003) 91-107.
[26] P. Norachan, S. Suthasupradit and K.-D. Kim, A co-rotational 8-node degenerated thin-walled element with assumed natural strain and enhanced assumed strain, *Finite Elements in Analysis and Design*, 50 (2012) 70-85.
[27] J. P. Pascon and H. B. Coda, Analysis of elastic functionally graded materials under large displacements via high-order tetrahedral elements, *Finite Elements in Analysis and Design*, 50 (2012) 33-47.
[28] L. Olovsson, M. Unosson and K. Simonsson, Selective mass scaling for thin walled structures modeled with tri-linear solid elements, *Computational Mechanics*, 34 (2004) 134-136.
[29] A. G. Olabi, E. Morris and M. S. J. Hashmi, Metallic tube type energy absorbers: A synopsis, *Thin-Walled Structures*, 45 (2007) 706-726.
[30] Z. Yao and K. J. R. Rasmussen, Material and geometric nonlinear isoparametric spline finite strip analysis of perforated thin-walled steel structures—Analytical developments, *Thin-Walled Structures*, 49 (2011) 1359-1373.
[31] W. Rust and K. Schweizerhof, Finite element limit load analysis of thin-walled structures by ANSYS (Implicit), LS-DYNA (explicit) and in combination, *Thin-Walled Structures*, 41 (2003) 227-244.
[32] A. Ahmed and L. J. Sluys, Implicit/explicit elastodynamics of isotropic and anisotropic plates and shells using a solid-like shell element, *European Journal of Mechanics - A/Solids*, 43 (2014) 118-132.
[33] M. Ortiz and E. P. Popov, Accuracy and stability of integration algorithms for elastoplastic constitutive relations, *International Journal for Numerical Methods in Engineering*, 21 (1985) 1561-1576.
[34] D. Owen and E. Hinton, *Finite elements in plasticity: Theory and practice*, Swansea: Pineridge Press (1980).
[35] F. Hildebrand, *Introduction to numerical analysis*, 2nd ed., Dover Publishers (1987).
[36] J. Marques, Stress computations in elastoplasticity, *Engineering with Computers*, 1 (1984) 42-51.
[37] M. Ortiz and J. C. Simo, An analysis of a new class of integration algorithms for elastoplastic constitutive relations, *International Journal for Numerical Methods in Engineerin*g, 23 (1986) 353-366.
[38] ASTM, *ASTM E8 / E8M - 13a*, West Conshohocken (2003).
[39] E. L. Guzas and C. J. Earls, Simulating blast effects on steel beam-column members: Methods, *Computers & Structures*, 89 (2011) 2133-2148.
[40] S. H. Paik, J. J. Moon, S. J. Kim and M. Lee, Parallel performance of large scale impact simulations on Linux cluster super computer, *Computers & Structures*, 84 (2006) 732-741.
[41] B. Ren and S. Li, Meshfree simulations of plugging failures in high-speed impacts, *Computers & Structures*, 88 (2010) 909-923.
[42] D. Notta-Cuvier, B. Langrand, E. Markiewicz, F. Lauro and G. Portemont, Identification of Johnson–Cook's viscoplastic model parameters using the virtual fields method: Application to titanium alloy Ti6Al4V, *Strain: An international Journal for Experimental Mechanics*, 49 (2013) 22-45.
[43] Hibbitt, Karlsson, Sorenson, *ABAQUS Theory Manual*, Pawtucket, RI, USA (1997).
[44] F. J. Harewood and P. E. McHugh, Comparison of the implicit and explicit finite element methods using crystal plasticity, *Computational Materials Science*, 39 (2007) 481-494.
[45] S.-Y. Chang, A new family of explicit methods for linear structural dynamics, *Computers & Structures*, 88 (2010) 755-772.
[46] *Analysis user's manual: Elements*, Dassault Systèmes Simulia Corp., Providence, RI, USA (2012).
[47] H. T. Y. Yang, S. Saigal and D. G. Liaw, Advances of thin shell finite elements and some applications—version I, *Computers & Structures*, 35 (1990) 481-504.
[48] E. Hinton and H. C. Huang, A family of quadrilateral Mindlin plate elements with substitute shear strain fields,

Computers & Structures, 23 (1986) 409-431.
[49] A. Acharya, A nonlinear generalization of the Koiter–Sanders–Budiansky bending strain measure, *International Journal of Solids and Structures*, 37 (2000) 5517-5528.
[50] F. Xu, G. Sun, G. Li and Q. Li, Experimental study on crashworthiness of tailor-welded blank (TWB) thin-walled high-strength steel (HSS) tubular structures, *Thin-Walled Structures*, 74 (2014) 12-27.
[51] M. White and N. Jones, Experimental quasi-static axial crushing of top-hat and double-hat thin-walled sections, *International Journal of Mechanical Sciences*, 41 (1999) 179-208.
[52] A. Prakash, E. Taciroglu and K. D. Hjelmstad, Computationally efficient multi-time-step method for partitioned time integration of highly nonlinear structural dynamics, *Computers & Structures*, 133 (2014) 51-63.
[53] C. Wood, A. J. Gil, O. Hassan and J. Bonet, Partitioned block-Gauss–Seidel coupling for dynamic fluid–structure interaction, *Computers & Structures*, 88 (2010) 1367-1382.
[54] E. Turan and P. Arbenz, Large scale micro finite element analysis of 3D bone poroelasticity, *Parallel Computing*, 40 (7) (2014) 239-250.
[55] I. M. Fonseca, P. M. Bainum and M. C. Santos, CPU time consideration for LSS structural/control optimization models with different degrees of freedom, *Acta Astronautica*, 54 (2004) 259-266.

Roozbeh Alipour received the B.S. and M.S. in Mechanical Engineering from Iran. He is currently is a Ph.D. candidate in Universiti Teknologi Malaysia and also lecturer in the Department of Mechanical Engineering of the Islamic Azad University, Mahshar Branch in Iran.

Ali Farokhi Nejad received the B.S. and M.S. in Mechanical Engineering from Iran and Universiti Teknologi Malaysia, respectively. He is currently is a Research Assistant in Universiti Teknologi Malaysia at Computational Solid Mechanics Laboratory.

Izman Sudin received the B.S. and M.S. and Ph.D in Mechanical and Industrial Engineering from Universiti Teknologi Malaysia and University of Warwick, UK. He is currently is a Associate Professor in the Faculty of Mechanical Engineering, Universiti Teknologi Malaysia.